frontiers | Frontiers in Earth Science

TYPE Brief Research Report
PUBLISHED 02 December 2025
DOI 10.3389/feart.2025.1720375

OPEN ACCESS

EDITED BY
Hao Shi,
Anhui University of Science and Technology, China

REVIEWED BY
Yongting Duan,
Northeastern University, China
Chong Liu,
The University of Hong Kong, Hong Kong SAR, China

*CORRESPONDENCE
Zhizhen Zhang,
zzzhang@cumt.edu.cn

RECEIVED 08 October 2025
REVISED 12 November 2025
ACCEPTED 17 November 2025
PUBLISHED 02 December 2025

CITATION
Zheng P, Xu K, Zhang H, Zhang Z, Qiang J, Zhang Y, Chen Q, Hu Y and Lai S (2025) Impact of fluids on the mechanical properties and fracturing behavior of deep reservoir rocks.
Front. Earth Sci. 13:1720375.
doi: 10.3389/feart.2025.1720375

Impact of fluids on the mechanical properties and fracturing behavior of deep reservoir rocks

Penglin Zheng[1], Ke Xu[1,2,3,4], Hui Zhang[1,2,3,4], Zhizhen Zhang[5]*, Jianli Qiang[1], Yu Zhang[1], Qiuyu Chen[1], Yixiong Hu[1] and Shujun Lai[1]

[1]PetroChina Tarim Oilfield Company, Korla, China, [2]Research and Development Center for Ultra-Deep Complex Reservoir Exploration and Development, China National Petroleum Corporation (CNPC), Korla, China, [3]Engineering Research Center for Ultra-deep Complex Reservoir Exploration and Development, Korla, China, [4]Xinjiang Key Laboratory of Ultra-deep Oil and Gas, Korla, China, [5]State Key Laboratory of Intelligent Construction and Healthy Operation and Maintenance of Deep Underground Engineering, School of Mechanics and Civil Engineering, China University of Mining and Technology, Xuzhou, China

The mechanical properties and fracturing behavior of deep reservoir rocks are significantly influenced by the presence of fluids, which is crucial for geomechanical evaluation and resource development efficiency. Based on a discrete element method (DEM) coupled with fluid-solid interaction modeling, this study systematically investigates the effects of different fluid types (water, oil, gas) and pore pressures on the mechanical characteristics and fracture evolution of rocks under deep reservoir conditions. The results indicate that fluid properties markedly alter the mechanical response of rocks. Water saturation induces the most significant deterioration in peak strength, with a degradation of 79.41% observed at a pore pressure of 120 MPa. In contrast, gas saturation leads to the greatest reduction in stiffness (Young's modulus), with a maximum degradation of 46.47% under the high pore pressure of 120 MPa. Increasing pore pressure considerably reduces rock strength, and its weakening effect surpasses that caused by varying fluid types. However, the influence of fluid type on stiffness is more pronounced than that of pore pressure. At the microscopic scale, water weakens intergranular cementation through physical wedging and hydration reactions, promoting the development of shear fractures. Oil, due to its higher viscous resistance, causes localized stress concentrations and accelerates failure. The high compressibility of gas primarily affects the deformation capacity. This study reveals the differential degradation mechanisms of rock strength and deformation parameters under multiphase fluid conditions, providing a theoretical basis for the safe development of deep oil and gas resources.

KEYWORDS

rock mechanics, fluid properties, pore pressure, mechanical properties, fracture

1 Introduction

Deep reservoirs host multiphase fluids such as petroleum, natural gas, and formation water. As typical fluid media, oil, gas, and water exhibit distinct physical properties,

including fluidity, dynamic viscosity, and compressibility modulus, which lead to variations in the mechanical characteristics and crack propagation patterns of fluid-bearing reservoir rocks. The chemical and mechanical interactions between fluids and rocks can impair permeability and porosity, ultimately altering petrophysical characteristics and creating operational challenges across various energy sectors, from enhanced oil recovery to gas storage operations (Karakul, 2018; Jafarbeigi and Moradi, 2025). Understanding the strength, deformation behavior, and fracture mechanisms of fluid-saturated rocks is crucial for the safe and efficient development of deep resources such as sandstone gas, shale gas and coalbed methane (Shi et al., 2022; Wu J. Y. et al., 2024; Yin et al., 2025; Wu et al., 2025a).

Recently, researchers have conducted extensive research on the mechanical characteristics and crack propagation behavior of fluid-bearing rocks, primarily focusing on laboratory experiments and numerical simulations (Zhang et al., 2021a; Yu et al., 2024; Zhang et al., 2024; Wu et al., 2025b). Due to the limitations of *in situ* testing applicability and the complexity of engineering geological conditions, laboratory testing remains the predominant approach in engineering practice. The advantages of laboratory experiments lie in their intuitiveness and ability to reflect actual engineering conditions (Bhuiyan et al., 2020; Zhang et al., 2021b; Liu et al., 2024). Significant experimental evidence has demonstrated the weakening effects of fluids on various rock types. For instance, water saturation consistently reduces compressive strength, tensile strength, and elastic modulus across different lithologies, as observed in mudstone (Jia et al., 2023; Teng et al., 2023), sandstone (Li et al., 2021), shale (Wang et al., 2019; Dabbaghi et al., 2024), igneous rock (Frolova et al., 2014), gypsum rock (Wang et al., 2020; Ji et al., 2025), phosphate rock (Li et al., 2023), and conglomerate (Duan et al., 2024). The degradation mechanism often involves physical deterioration, chemical erosion, and mechanical damage, with the degree of alteration depending on mineral composition and cementation characteristics (Zhong et al., 2019; Liao et al., 2020; Deng et al., 2023). Beyond water saturation, studies have revealed that different fluid types induce distinct mechanical responses. The impact of drilling fluids on hard brittle shale further demonstrates how different fluid systems alter rock structure and chemical properties, ultimately affecting borehole stability (Huang et al., 2019; Karakul, 2021). In carbonate reservoirs, different fracturing fluids exhibit discrepant impact degrees, with gelled acid causing the most significant deterioration of physical and mechanical properties (Deng et al., 2023).

Numerical simulation offers complementary advantages such as low cost, high repeatability, facilitated observation of internal characteristic fields, and quantitative analysis of micromechanical fracture mechanisms (Zhao et al., 2021). Advanced numerical methods including the finite element method (FEM) with phase-field modeling of rock fractures (Fei et al., 2022), finite volume method (FVM) with hybrid approaches for hydraulic fracturing (Liu et al., 2018), and discrete element method (DEM) have effectively addressed limitations of laboratory core experiments (Shi et al., 2023; Yao et al., 2024; Shi et al., 2025). Micro-scale hydro-mechanical modeling has proven valuable for predicting transport properties of deformed natural fractures and understanding the important role of fracture parameters on transport behavior (Raziperchikolaee et al., 2014). Particularly for fluid-particle systems, the coupled computational fluid dynamics (CFD) and discrete element method (DEM) approach has proven effective in accurately simulating various fluid-particle interaction problems (Xu et al., 2024). Researchers have successfully utilized particle flow code (PFC) to study fracture evolution during hydraulic fracturing, incorporating seepage-stress coupling effects to simulate fracture propagation (Shi et al., 2025; Wang et al., 2014). Recent numerical investigations have also explored the impact of water-rock interactions on the propagation of water-flooding induced fractures, revealing how alterations in geomechanical properties affect fracture propagation under reservoir conditions (Qu et al., 2023).

Numerous scholars have conducted extensive mechanical experiments and hydraulic fracturing simulations on fluid-bearing rocks, particularly those under varying water saturation conditions. However, research on oil- and gas-bearing rocks remains insufficient, and studies on the triaxial compression mechanical behavior of fluid-saturated rocks using DEM coupled with fluid-solid interaction (FSI) methodologies are relatively limited. The coupled CFD and DEM approach has proven effective in accurately simulating various fluid-particle interaction problems (Xu et al., 2024). Therefore, this study employs a discrete element-based fluid-solid coupling method to perform triaxial compression simulations on deep reservoir rocks containing different pore fluids, aiming to investigate the mechanical properties and fracture mechanisms of reservoir rocks under varying fluid occurrence conditions.

2 Numerical simulation methods for fluid-solid coupling in fluid-bearing rocks

2.1 Fluid-solid coupling simulation methodology

In Particle Flow Code (PFC), the constitutive behavior of materials is simulated through contact models between particles. This study primarily employs the Parallel Bond Model (PBM) to simulate the mechanical behavior of rock particles. The PBM establishes a finite-sized bonding area at the particle contact surface to resist normal forces (F_n), tangential forces (F_s), and bending moments (M). Bond failure is determined based on strength criteria (normal strength σ_c, tangential strength τ_c).

In the discrete element method, the voids between particles are typically treated as rock pores, with fluid flow realized through a pore-throat network. The centroids of adjacent particles are connected to form polygonal fluid domains. These adjacent fluid domains are interconnected through throats (i.e., bonded contacts between particles). Individual polygonal fluid domains are interconnected through flow channels, forming a comprehensive fluid network model. Within this model, the fluid stored in each domain represents an abstract virtual entity. A pressure difference exists between adjacent fluid domains, driving fluid flow and exchange through interconnecting channels. The flow rate (q) through these channels is governed by the cubic law (Zhang et al., 2018):

$$q = \frac{1}{12\mu} a^3 \frac{P_2 - P_1}{L} t$$

where q is the fluid flow rate through the channel per unit time; μ is the dynamic viscosity of the fluid; a is the aperture of the flow

channel; P_1 and P_2 are the pore pressures in the two adjacent fluid domains; L is the length of the flow channel, calculated as $L = r_1 + r_2$, where r_1 and r_2 are the radii of the two adjacent particles; t is the thickness of the specimen (flow channel). As a two-dimensional model is used, $t = 1$.

To simplify the calculation, the length of the flow channel L is defined as the sum of the radii of the two particles at the bonded contact of the current channel, i.e., $L = r_1 + r_2$. The aperture a of the flow channel represents the gap between the surfaces of two adjacent particles. The magnitude of a is influenced by the magnitude and type of the normal contact force F between the two particles. Assuming a_0 is the initial aperture in the absence of contact force, then:

When F is a compressive stress,

$$a = \frac{a_0 F_0}{F + F_0}$$

where F_0 is the normal contact force at which the aperture decreases to half of its initial value a_0. When $F = 0$, the aperture $a = a_0$; When $F = F_0$, the aperture $a = a_0/2$; As F approaches infinity, the aperture a asymptotically approaches zero.

When F is a tensile stress,

$$a = a_0 + \lambda(d - r_1 - r_2)$$

where d is the distance between the centers of the two particles; r_1 and r_2 are the radii of the two particles, respectively; λ is a dimensionless coefficient. For most models, the particle radii are typically much larger than the actual mineral grain sizes in real rock specimens. Consequently, the calculated aperture tends to be overestimated. Therefore, an adjustment coefficient λ is introduced to obtain a reasonable aperture value. The value of λ is generally less than 1.

The change in fluid pressure within a fluid domain is determined by both the domain volume change ΔV_d and the fluid bulk modulus K_f. During a time step Δ_t, if the net flow rate into the domain through connected channels is Σq, then the change in fluid pressure Δp within the domain is given by:

$$\Delta p = \frac{K_f}{V_d}(\Sigma q \Delta t - \Delta V_d)$$

where V_d is the volume of the fluid domain.

2.2 Selection of rock and fluid property parameters

To ensure the accuracy of the rock model, the micro-parameters were calibrated against laboratory triaxial compression tests reported in the literature for deep reservoir sandstones (Wu Q. Q. et al., 2024;). The "trial-and-error" method was then employed to iteratively adjust the micro-parameters (e.g., particle stiffness, bond strength) until the numerical model's macroscopic response closely matched these experimental benchmarks. Based on the influence of elastic modulus (E), cohesion (c), tensile strength (σ_t), and internal friction angle (fa) on the strength of the rock model, repeated trial calculations and adjustments were performed according to experimental results to obtain model data that closely matches the laboratory experimental results. Three types of fluids, including water, oil, and gas, are considered. The differentiation among fluids primarily considers their compressibility, dynamic viscosity, and mobility. By specifying numerical values for these three fluid parameters, the model simulates the realistic physicochemical interactions between different fluids and rock particles. The model parameter settings are listed in Table 1. This set of data was used for simulating the mechanical properties and fracture patterns of rocks under different fluid occurrence conditions. Water is modeled as a slightly compressible fluid with low viscosity, typical of formation water. Oil is represented as a light crude oil, characterized by a moderate viscosity that is significantly higher than that of water and gas, leading to greater viscous resistance during flow. Gas is modeled as natural gas (e.g., methane), with its key characteristics being very low viscosity and high compressibility. It should be noted that the gas phase is modeled as a non-reactive fluid. While we recognize the potential importance of phenomena such as the Klinkenberg effect and gas dissolution in pore water for specific reservoir scenarios, these are not explicitly incorporated in the current model. This approach is justified as our primary aim is to isolate and compare the first-order mechanical influences of fundamental fluid properties on rock behavior.

2.3 Model establishment

The rock model in this study was generated by centrally packing ball particles within a domain region of height 200 mm × width 100 mm. The rock specimen dimensions were set to height 100 mm × width 50 mm. The ball particle diameters were randomly generated within the range of 0.8–1.2 mm, with a uniform particle density of 2,660 kg/m^3. A local damping coefficient of 0.5 was applied uniformly. The normal stiffness between particles was set to 32 GPa, while the linear stiffness between particles and walls was set to 16 GPa, with a stiffness ratio of 2.0 for both. The friction coefficient was set to 0.6 for all contacts. Initial porosity values were set to 0.01, 0.05, and 0.10, resulting in the generation of 6,213, 5,963, and 5,639 ball particles, respectively. The pore pressures were initialized to 10 MPa, 80 MPa, and 120 MPa, respectively, uniformly throughout the specimen's fluid domains. Un drained hydraulic boundary conditions were applied, meaning no fluid flow was permitted across the model boundaries during compression. This setup simulates a rapid loading process where fluid exchange with the external environment is negligible. Consequently, the pore pressure evolved dynamically during loading in response to volumetric strain.

A constant confining pressure of 150 MPa was applied to all models to simulate deep reservoir conditions. The pre-compaction process eliminates initial particle overlaps through servo control and establishes a homogeneous stress field, bringing the particle system to a state of static equilibrium. At this stage, particles maintain only point contacts (linear contact model), which can transmit forces and damping but cannot resist bending moments or torques, thereby simulating the behavior of non-cohesive granular materials (e.g., sand). After adding parallel bonds (linear parallel bonds), finite-sized bonding surfaces (equivalent to cementation layers) form between particles. These bonds can transmit forces, bending moments, and torques, endowing the particle system with tensile

TABLE 1 Parameter settings for numerical models of rocks and different fluids.

Parameter			Value			
Name	Notation	Unit	Water-saturated state	Oil-saturated state	Gas-saturated state	Dry state
Elastic modulus	E	GPa	16.0	19.0	12.0	21
Elastic modulus_pb	E_pb	GPa	32.0	38.0	24.0	42
Stiffness ratio	Sr	—	2.0	2.0	2.0	2.0
Tensile strength	σ_t	MPa	5.0	7.8	8.2	10.0
Cohesion	c	MPa	30.0	49.0	50.3	60.0
Internal friction angle	fa	°	30.0	40	41	45
Dynamic viscosity	μ	Pa·s	1e-3	1e-2	1.1e-5	—
Compression modulus	K	GPa	2.0	1.2	0.2	—
Mobility	λ	mD/(mPa·s)	1e-3	1e-4	9.09e-2	—

strength (pb_ten) and shear cohesion (pb_coh), thus simulating the continuum behavior of rocks or concrete. If bonds are added before pre-compaction, the excessive contact forces caused by particle overlaps would instantly break the bonds, generating non-physical cracks and compromising the homogeneity of the specimen. After pre-compaction, particle positions stabilize, ensuring accurate calculation of bond areas (pb_radius) and preventing bond size distortion due to particle displacement. This approach establishes a parallel bond model (PBM) with realistic physical properties of rock to simulate mechanical behavior. The reliability of this model for simulating rock mechanical behavior has been validated by Sun (Sun and Wang, 2024) and Wang (Wang and Wang, 2021).

The two-dimensional (2D) modeling approach has certain limitations. Fluid flow and fracture propagation are confined to a single plane, which simplifies the true three-dimensional characteristics of the rock pore network and fluid pathways, hindering the simulation of the complexity and connectivity of out-of-plane fractures. Although these simplifications mean that the absolute values of strength, permeability, and fracture geometry may not directly correspond to field conditions, two-dimensional models offer significant computational advantages for large-scale parametric studies. The main objective of this study—identifying and comparing the relative effects of different pore fluids on rock mechanical behavior and their distinct mechanisms—can be effectively achieved using this model.

3 Numerical simulation results

3.1 Stress-strain curves and mechanical parameters

Variations in fluid pore pressure and rock porosity significantly influence the mechanical properties and crack propagation behavior of rocks under fluid-bearing conditions. Porosity is defined as the ratio of pore volume to the total rock volume, with fluids primarily residing within these pores. Pore pressure refers to the pressure exerted by the fluid within the rock pores, whose magnitude depends on fluid density and vertical depth. The level of pore pressure is a critical factor affecting rock strength; generally, an increase in pore pressure reduces the effective stress on the rock skeleton, thereby weakening the rock strength. This study simulates the triaxial compression mechanical processes of fluid-saturated rocks under multiple pore pressure and porosity levels for different fluids (oil, gas, water).

Figure 1 presents the simulated stress-strain curves of rocks under different fluid occurrence conditions. To clearly illustrate the influence of varying pore pressures and initial porosity combinations on rock mechanical properties, the simulation provides results from nine sets of stress-strain curves. It can be observed that the effects of different fluid types on rock mechanical properties are evident. When the pore pressure is low (Pp = 10 MPa), the effective confining pressure is high, and the influence of different fluid properties on peak strength is relatively similar. The degree of strength degradation follows the order: water-saturated > gas-saturated ≈ oil-saturated. In contrast, the impact of fluid properties on Young's modulus varies significantly, with stiffness degradation following the sequence: gas-saturated > water-saturated > oil-saturated. When the pore pressure is equal to 80 MPa, the effective stress gradually decreases. Strength degradation still follows the pattern: water-saturated > gas-saturated ≈ oil-saturated, while stiffness degradation remains consistent: gas-saturated > water-saturated > oil-saturated. As pore pressure increases (up to 120 MPa), effective stress further decreases, and the weakening effect of different fluids on rock strength becomes significantly distinct, following the order: water-saturated > oil-saturated > gas-saturated. Stiffness degradation adheres to the pattern: gas-saturated > water-saturated > oil-saturated.

Under dry conditions, the rock exhibits a peak strength of 505 MPa and an elastic modulus of 70.22 GPa. Under identical confining pressure but varying pore pressures, water saturation

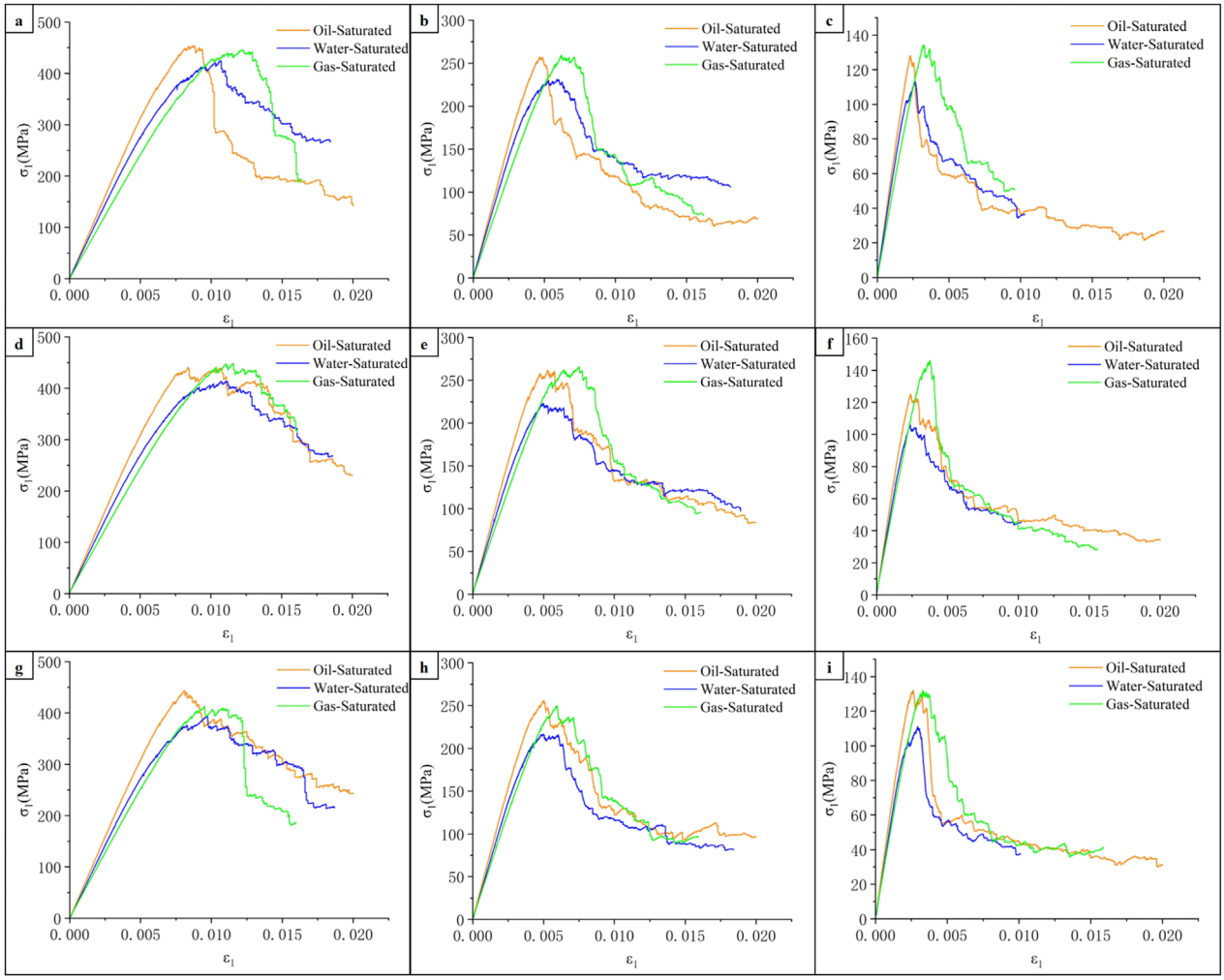

FIGURE 1
Stress-Strain curves of Rocks Under Different Fluid Properties. (**(a)** Porosity = 0.01, Pp = 10 MPa; **(b)** Porosity = 0.01, Pp = 80 MPa; **(c)** Porosity = 0.01, Pp = 120 MPa; **(d)** Porosity = 0.05, Pp = 10 MPa; **(e)** Porosity = 0.05, Pp = 80 MPa; **(f)** Porosity = 0.05, Pp = 120 MPa; **(g)** Porosity = 0.1, Pp = 10 MPa; **(h)** Porosity = 0.1, Pp = 80 MPa; **(i)** Porosity = 0.1, Pp = 120 MPa).

induces the most severe degradation in peak strength. When the pore pressure reaches 120 MPa, the peak strength is reduced to 104 MPa, corresponding to a degradation of 79.41%. In contrast, gas saturation causes the most significant reduction in stiffness, with the Young's modulus of the gas-saturated rock decreasing to 37.59 GPa, representing a degradation of 46.47%. Note that the reported percentage degradation of peak strength and Young's modulus is calculated by comparing the values of fluid-saturated samples with those of the dry rock sample under the same confining pressure.

An increase in initial porosity always leads to a decrease in peak strength and Young's modulus under various fluid types and pore pressure conditions. This occurs because a higher porosity implies a greater proportion of weak pores in the rock matrix and a reduced load-bearing solid area, thereby facilitating failure and enhancing compressibility. Although the qualitative trend is consistent, the quantitative weakening effect induced by porosity variation is generally less pronounced than that caused by high pore pressure or the presence of fluids.

3.2 Force chains, particle displacement and velocity

The simulation employed a single-stage loading process with a strain rate of 0.8×10^{-3}/s, satisfying quasi-static loading conditions (Huang et al., 2016). The loading process automatically terminated, and the model state was saved when the axial strain reached 0.02. Figure 2 compares the force chains, cracks, displacement, and velocity of rock particles under different fluid types at an axial strain of 0.02. At this point, the rock has already been compressed to failure. All force chains are under compression, as they cannot transmit tensile stress. Sparse force chain regions correspond to crack distribution zones, indicating severe bond failure. The water-saturated rock sample exhibits sparser force chains, reflecting more extensive damage. The number of shear cracks in the water-saturated rock sample is significantly higher than in the gas- and oil-saturated rock samples. The presence of water more noticeably weakens the cementation strength of the rock, making it more prone to shear failure. The particle velocity is highest

in the gas-saturated rock sample, followed by the water-saturated rock sample, and lowest in the oil-saturated rock sample. This indicates that the high dynamic viscosity of oil significantly hinders particle movement, resulting in relatively higher rock stiffness in the oil-saturated state compared to other fluid conditions. Particle displacement and velocity vector maps also reflect crack distribution patterns. Greater particle displacement correlates with higher crack density, while opposing, intersecting, or disordered particle velocity directions are more likely to form fracture zones.

3.3 Crack evolution

In the Parallel Bond Model, the failure of a bond is classified as either a tensile crack or a shear crack at the moment of rupture. A tensile crack is registered if the maximum tensile stress in the bond reaches its specified tensile strength. A shear crack is registered if the shear stress in the bond exceeds its shear strength, which is governed by a Mohr-Coulomb criterion defined by the bond cohesion and friction angle. This intrinsic classification mechanism of the PBM allows for the direct tracking of micro-crack types during the simulation. Figure 3 shows the evolution curves of crack numbers under different fluid conditions. The deformation and failure of rocks under triaxial compression exhibit typical stage-specific characteristics, which can generally be divided into five distinct phases: compaction stage, elastic deformation stage, plastic yield stage (stable crack propagation stage), strain softening stage (unstable crack propagation stage), and residual plastic stage (plastic flow stage) (Li et al., 2024; Wang et al., 2024). During the elastic deformation stage (when ε_1 is relatively small), the growth rate of cracks is slow, and the crack types are primarily tensile cracks, with very few shear cracks. In the plastic yield stage, the number of tensile and shear cracks increases rapidly, particularly in the water-saturated state. After reaching the peak stress, the growth rate of tensile cracks reaches its maximum, while the number of shear cracks stabilizes, either growing slowly or remaining unchanged. During the strain softening and residual stages, the growth rate of tensile cracks slows down, and shear cracks remain largely unchanged. The rock ultimately fails due to the interconnection of cracks.

Overall, the gas-saturated rock sample exhibits the fewest cracks. Combined with the fact that gas causes the least degradation of rock strength, it can be concluded that gas has the smallest weakening effect on the rock's resistance to fracture. In contrast, the water-saturated rock sample shows the highest number of cracks, with shear cracks significantly outnumbering those in the gas- and oil-saturated rock samples. This indicates that water makes the rock more prone to shear slip failure. Furthermore, the crack initiation stress, propagation stress, and peak stress all follow the order: water-saturated < oil-saturated < gas-saturated. This suggests that cracks initiate and propagate more easily in the water-saturated state compared to the oil- and gas-saturated states.

4 Discussion

Figure 4 shows the point-line diagrams of the degradation trends for peak strength and Young's modulus of rocks. As the pore pressure increases, the strength degradation under gas-saturated condition ranges from 11.09% to 71.09%, and modulus degradation ranges from 42.11% to 46.47%; under oil-saturated condition, strength degradation ranges from 12.67% to 75.25%, and modulus degradation ranges from 8.72% to 14.21%; Under water-saturated condition, strength degradation ranges from 18.02% to 79.41%, and modulus degradation ranges from 23.27% to 29.85%. Under the same stress conditions, the strength degradation follows the order: water-saturated > oil-saturated > gas-saturated, while the Young's modulus degradation follows: gas-saturated > water-saturated > oil-saturated.

The presence of fluids weakens the Young's modulus of the rock, but as pore pressure increases, the extent of modulus reduction decreases. The weakening effect of increasing pore pressure on rock strength is greater than that caused by changes in fluid type. Conversely, the weakening effect of fluid type changes on rock stiffness is greater than that caused by increasing pore pressure.

Fluid-solid coupling interactions are influenced by effective stress and fluid properties. The effective stress is determined by the confining pressure and pore pressure, while fluid properties are generally affected by dynamic viscosity, permeability, and fluid bulk modulus. Under fluid pressure, free water flows from pore throats into the pores, eventually saturating the entire rock. The presence of fluids increases the number and size of pores, leading to an increase in internal porosity. An increase in fluid pressure (pore pressure) reduces the effective stress, resulting in the weakening of rock strength due to fluid saturation. When the rock is fully saturated with fluid, the fluid within the pores affects the interparticle cohesion by increasing the particle spacing D, thereby influencing the overall strength.

Water molecules exert physical wedging effects and hydration reactions on rock mineral particles. The penetration of water molecules into intergranular spaces significantly reduces the cementation strength between rock particles. This is particularly pronounced in rocks with higher clay content, as clay minerals are more susceptible to alteration upon rock/fluid interaction, leading to greater strength degradation (Zhong et al., 2019). Simultaneously, the presence of water induces swelling in certain mineral components, leading to structural deterioration of the rock fabric. Experimental studies on clay-bearing sandstones have confirmed that the degree of weakening depends on the clay composition, with water causing more significant strength reduction in rocks containing swelling clays like montmorillonite compared to those with only kaolinite (Wu et al., 2024;). As a result, the overall load-bearing capacity of the rock is compromised. In contrast, gas molecules are smaller and exhibit lower dynamic viscosity. They primarily exist in a free state within rock pores and have limited influence on interparticle forces. The impact of oil on the peak stress of rock lies between that of water and gas. Due to its higher viscosity compared to water and gas, oil generates considerable viscous resistance when flowing through rock pores under external stress. This resistance leads to non-uniform stress distribution and localized stress concentrations within the rock, thereby promoting premature failure and reducing the peak stress. The investigation of fracture properties under drilling fluid saturation also suggests that fluids can alter the rock's resistance to fracture propagation, with the viscous nature of the fluid playing a role (Karakul, 2021; Zhang et al., 2022; Xu et al., 2023).

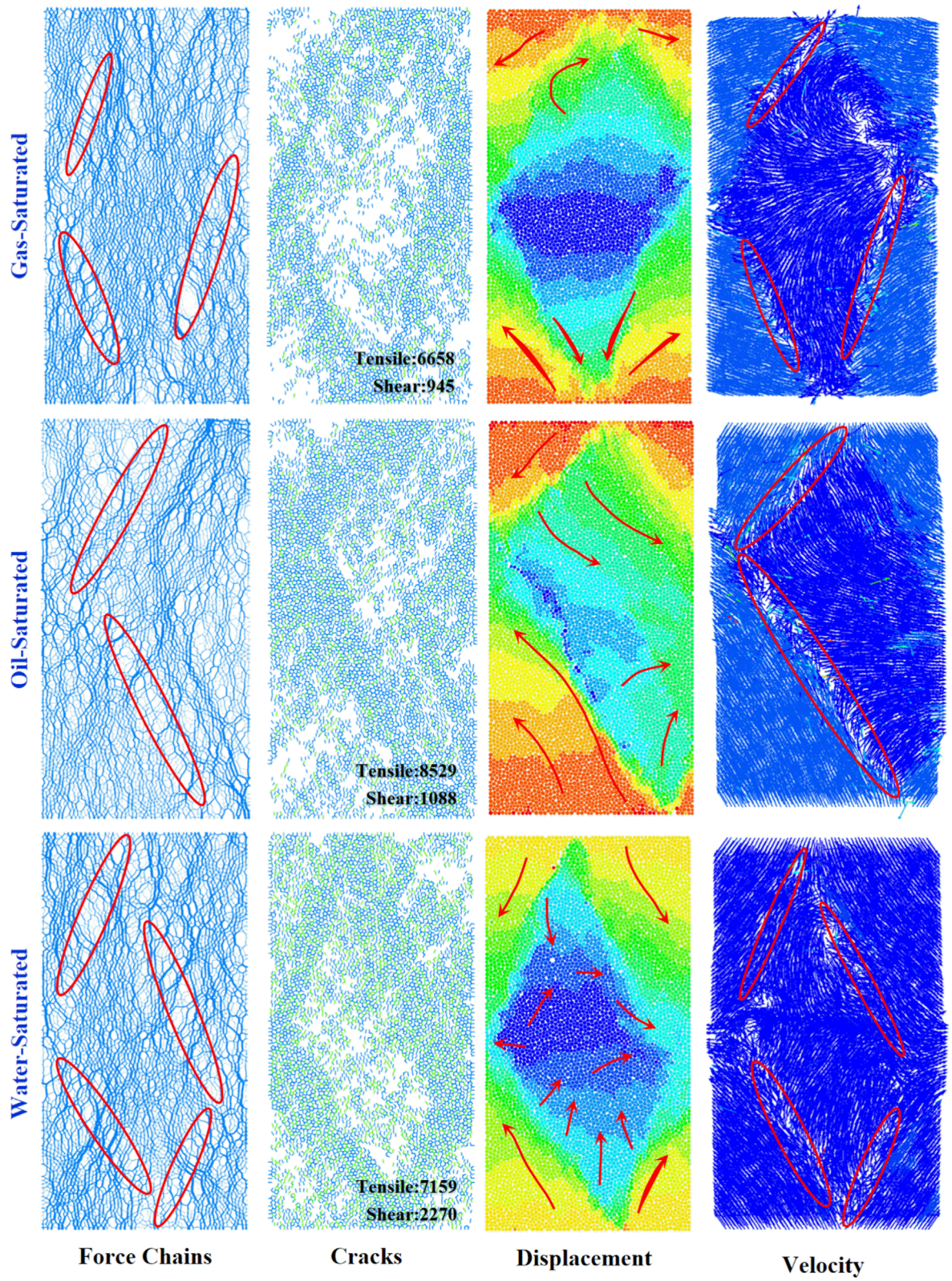

FIGURE 2
Force Chains, Crack Distribution, Particle Displacement, and Velocity Nephograms under Different Fluid Conditions. (Porosity: 0.05, Pore pressure: 10 MPa).

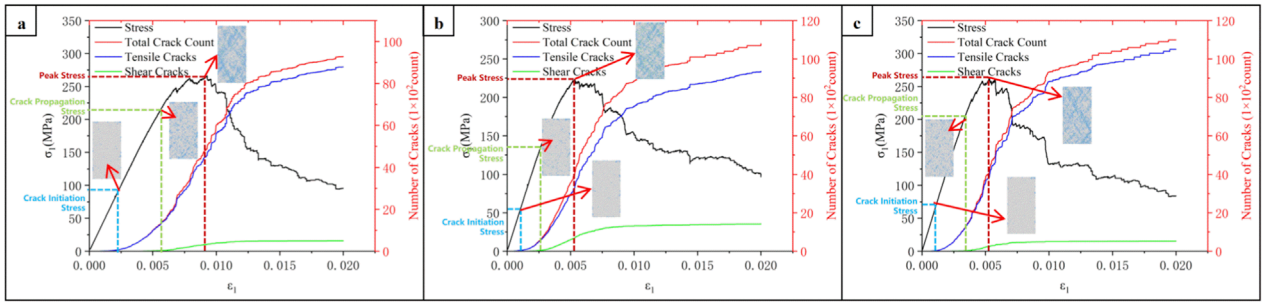

FIGURE 3
Variation curves of crack numbers under different fluid conditions. (porosity: 0.05, pore pressure: 80 MPa); ((**a**) Gas-Saturated State; **(b)** Water-Saturated State; **(c)** Oil-Saturated State).

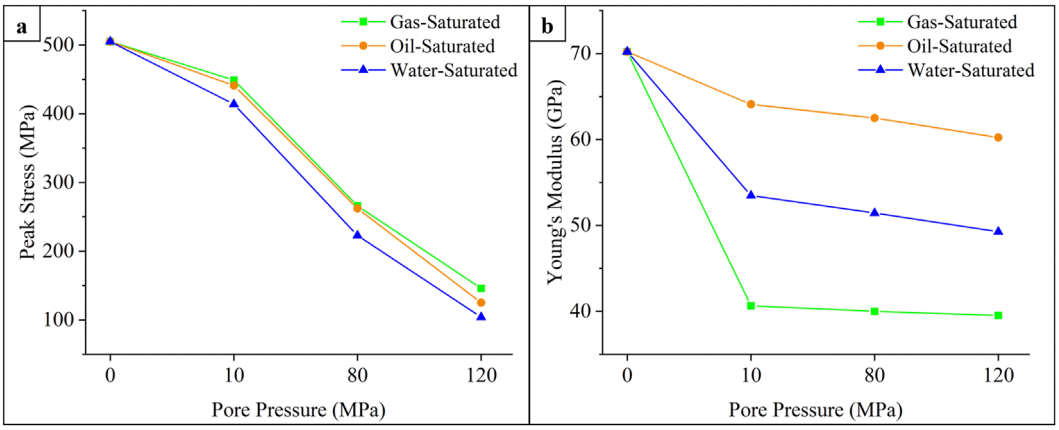

FIGURE 4
Trend diagram of rock mechanical property degradation. ((**a**) Relationship between peak stress and pore pressure in rocks under different fluid conditions; **(b)** Relationship between Young's modulus and pore pressure in rocks under different fluid conditions).

The high compressibility of gas is identified as the dominant mechanism for its maximum reduction of Young's modulus. During the initial elastic compression, the applied load causes volumetric strain. The highly compressible gas within the pores offers minimal resistance to this pore volume reduction, unlike the nearly incompressible water. Consequently, a greater proportion of the applied work is converted into compressing the gas-filled pores rather than elastically straining the solid rock skeleton. Studies on gas-containing coal and tight sandstones interacting with $scCO_2$ have similarly shown that the highly compressible gas phases offer minimal resistance to pore volume reduction during compression, leading to increased overall compressibility and a lower apparent Young's modulus (Zhang et al., 2021a; Yang et al., 2023).

The weakening trends observed in this study align with the broader understanding that fluid-rock interactions can significantly deteriorate the physical and mechanical properties of rocks across various lithologies and engineering contexts, from hydraulic fracturing to geological storage (Jafarbeigi and Moradi, 2025; Bhuiyan et al., 2020). The differential weakening mechanisms highlighted here—where water primarily attacks cementation strength and gas compromises stiffness via compressibility—provide a micro-mechanical explanation for the macro-scale observations of fluid-induced alterations in reservoir rocks.

5 Conclusion

This study investigates the deep reservoir rocks of the Kuqa Depression through PFC discrete element numerical simulations, the mechanical characteristics and crack evolution patterns of fluid-bearing reservoir rocks were analyzed from multiple perspectives, including stress-strain curves, force chains, particle displacement, and crack propagation. The main findings are as follows:

1. The rock strength degradation follows the order: water-saturated > oil-saturated > gas-saturated, water causes the most significant strength degradation in rocks. The weakening effect of pore pressure on rock strength is greater than that caused by changes in fluid type. Fluid type, pore pressure, and porosity all influence rock strength, with pore pressure variation having the most significant impact.
2. The Young's modulus degradation follows the order: gas-saturated > water-saturated > oil-saturated, indicating that gas

has the most significant impact on the rock's resistance to deformation. Changes in fluid type have a greater weakening effect on rock stiffness than increases in pore pressure.

1. At rock failure, the stress chains are exclusively compressive. Under water-saturated conditions and high pore pressure states, the force chains become sparser, indicating more severe rock damage. From gas-saturated to water-saturated to oil-saturated states, the instantaneous particle velocity gradually decreases, attributable to the higher dynamic viscosity of oil, which hinders particle movement.
2. The number of shear cracks in the water-saturated state is significantly higher than in the gas- and oil-saturated states. The presence of water more noticeably weakens the cementation strength of the rock, making it more prone to shear failure.

Data availability statement

The original contributions presented in the study are included in the article/supplementary material, further inquiries can be directed to the corresponding author.

Author contributions

PZ: Writing – original draft, Data curation. KX: Investigation, Writing – original draft, Funding acquisition, Conceptualization. HZ: Supervision, Resources, Validation, Writing – original draft. ZZ: Writing – review and editing, Methodology, Conceptualization, Funding acquisition. JQ: Writing – review and editing, Data curation, Investigation. YZ: Writing – review and editing, Resources, Formal Analysis. QC: Writing – review and editing, Software, Visualization. YH: Visualization, Software, Writing – review and editing. SL: Writing – review and editing, Data curation, Investigation.

Funding

The authors declare that financial support was received for the research and/or publication of this article. This research was funded by the National Natural Science Foundation of China (Nos. 42030810, 52174091), and the National Science and Technology Major Project (No. 2025ZD1400500).

Acknowledgements

We express our gratitude to the editors and reviewers for their dedication and hard work.

Conflict of interest

Authors PZ, KX, HZ, JQ, YZ, QC, YH, and SL were employed by PetroChina Tarim Oilfield Company. Authors KX, and HZ were employed by China National Petroleum Corporation (CNPC).

The remaining author declare that the research was conducted in the absence of any commercial or financial relationships that could be construed as a potential conflict of interest.

Generative AI statement

The authors declare that no Generative AI was used in the creation of this manuscript.

Any alternative text (alt text) provided alongside figures in this article has been generated by Frontiers with the support of artificial intelligence and reasonable efforts have been made to ensure accuracy, including review by the authors wherever possible. If you identify any issues, please contact us.

Publisher's note

References

Bhuiyan, M. H., Agofack, N., Gawel, K. M., and Cerasi, P. R. (2020). Micro- and macroscale consequences of interactions between CO2 and shale rocks. *Energies* 13 (5), 1167. doi:10.3390/en13051167

Dabbaghi, E., Ng, K., Kou, Z., Copeland, G., and Alvarado, V. (2024). Experimental investigation to understand the effect of fracturing fluid on the geomechanical behavior of mowry shale. *J. Petroleum Explor. Prod. Technol.* 14 (6), 1505–1519. doi:10.1007/s13202-024-01788-6

Deng, P., Guo, Y. T., Zhou, J., Wang, L., Zhou, X., and Xu, F. (2023). An experimental investigation of fracturing fluids on physico-mechanical damage properties of carbonates in block Shunbei. *Energy Sources Part A-Recovery Util. Environ. Eff.* 45 (4), 11060–11081. doi:10.1080/15567036.2019.1683648

Duan, X. L., Zhang, Q., Cao, Y. J., Zhao, D. F., Wang, W., Zhu, Q. Z., et al. (2024). Study on water sensitivity effect and mechanical damage characteristics of xiyu conglomerate under complex water environment and stress conditions. *Chin. J. Rock Mech. Eng.* 43 (12), 2992–3004. doi:10.13722/j.cnki.jrme.2024.0312

Fei, F., Choo, J., Liu, C., and White, J. A. (2022). Phase-field modeling of rock fractures with roughness. *Int. J. Numer. Anal. Methods Geomechanics* 46 (5), 841–868. doi:10.1002/nag.3317

Frolova, J., Ladygin, V., Rychagov, S., and David, Z. (2014). Effects of hydrothermal alterations on physical and mechanical properties of rocks in the Kuril-Kamchatka island arc. *Eng. Geol.* 183, 80–95. doi:10.1016/j.enggeo.2014.10.011

Huang, Y., Yang, S., and Zeng, W. (2016). Experimental and numerical study on loading rate effects of rock-like material specimens containing two unparallel fissures. *J. Central South Univ.* 23 (06), 1474–1485. doi:10.1007/s11771-016-3200-3

Huang, T., Cao, L. N., Cai, J. J., and Xu, P. (2019). Experimental investigation on rock structure and chemical properties of hard brittle shale under different drilling fluids. *J. Petroleum Sci. Eng.* 181, 106185. doi:10.1016/j.petrol.2019.106185

Jafarbeigi, E., and Moradi, S. S. T. (2025). The influence of fluids on the petrophysical and mechanical properties of rocks in enhanced oil recovery and gas storage operations: a holistic review. *J. Petroleum Explor. Prod. Technol.* 15 (11), 170. doi:10.1007/s13202-025-02093-6

Ji, Y. K., Ji, H. J., Wu, L., Yang, C., and Vandeginste, V. (2025). Gypsum rock and water/crude oil interaction during crude-oil storage in abandoned gypsum mine. *Rock Mech. Rock Eng.* 58 (7), 7819–7834. doi:10.1007/s00603-025-04546-0

Jia, R., Fu, X. F., Jin, Y. J., Wu, T., Wang, S., and Cheng, H. (2023). Mechanical properties of mudstone caprock and influencing factors: implications for evaluation of caprock integrity. *Front. Earth Sci.* 11, 1229851. doi:10.3389/feart.2023.1229851

Karakul, H. (2018). Effects of drilling fluids on the strength properties of clay-bearing rocks. *Arabian J. Geosciences* 11 (16), 450. doi:10.1007/s12517-018-3816-8

Karakul, H. (2021). Investigation of fracture properties of rocks under drilling fluid saturation. *Environ. Earth Sci.* 80 (15), 496. doi:10.1007/s12665-021-09792-3

Li, H., Qiao, Y., Shen, R., He, M., Cheng, T., Xiao, Y., et al. (2021). Effect of water on mechanical behavior and acoustic emission response of sandstone during loading process: phenomenon and mechanism. *Eng. Geol.* 294, 106386. doi:10.1016/j.enggeo.2021.106386

Li, S. J., Wang, C. Y., Zhang, D. M., Wang, M., Zhou, F., and Pan, Y. (2023). Deterioration mechanism of mechanical properties of phosphorite under different saturation duration. *Front. Earth Sci.* 11, 1227742. doi:10.3389/feart.2023.1227742

Li, M. F., Liang, J. W., and Dou, Y. H. (2024). Experimental study on mechanical properties of rock in water-sensitive oil and gas reservoirs under high confining pressure. *Appl. Sciences-Basel* 14 (24), 11478. doi:10.3390/app142411478

Liao, Z. H., Wu, M. N., Chen, X. F., and Zou, H. (2020). Fracture mechanical properties of carbonate and evaporite caprocks in Sichuan basin, China with implications for reservoir seal integrity. *Mar. Petroleum Geol.* 119, 104468. doi:10.1016/j.marpetgeo.2020.104468

Liu, C., Shen, Z. Z., Gan, L., Jin, T., Zhang, H., and Liu, D. (2018). A hybrid finite volume and extended finite element method for hydraulic fracturing with cohesive crack propagation in quasi-brittle materials. *Materials* 11 (10), 1921. doi:10.3390/ma11101921

Liu, X. W., Chen, J. X., Liu, B., Wang, S., Liu, Q., and Luo, J. (2024). Effects of seepage pressure on the mechanical behaviors and microstructure of sandstone. *J. Rock Mech. Geotechnical Eng.* 16 (6), 2033–2051. doi:10.1016/j.jrmge.2023.09.010

Qu, H. Y., Peng, Y., Pan, Z. J., Xu, X., and Zhou, F. (2023). Numerical study on the impact of water-rock interactions on the propagation of water-flooding induced fracture. *Front. Earth Sci.* 11, 1129913. doi:10.3389/feart.2023.1129913

Raziperchikolaee, S., Alvarado, V., and Yin, S. (2014). Prediction of transport properties of deformed natural fracture through micro-scale hydro-mechanical modeling. *Transp. Porous Media* 104 (1), 1–23. doi:10.1007/s11242-014-0317-4

Shi, H., Song, L., Zhang, H. Q., Chen, W. L., Lin, H. S., Lin, D. Q., et al. (2022). Experimental and numerical studies on progressive debonding of grouted rock bolts. *Int. J. Min. Sci. Technol.* 32 (1), 63–74. doi:10.1016/j.ijmst.2021.10.002

Shi, H., Chen, W. L., Zhang, H. Q., Song, L., Li, M., Wang, M., et al. (2023). Dynamic strength characteristics of fractured rock mass. *Eng. Fract. Mech.* 292, 109678. doi:10.1016/j.engfracmech.2023.109678

Shi, H., Chen, W. L., Wu, J. Y., Chuanxin, R., Zhenshuo, W., lei, S., et al. (2025). Unified rock strength theory incorporating holistic consideration of macro-meso-micro defect coupling effects. *Eng. Fract. Mech.* 328, 111534. doi:10.1016/j.engfracmech.2025.111534

Sun, R., and Wang, J. (2024). Effects of *in situ* stress and multiborehole cluster on hydraulic fracturing of shale gas reservoir from multiscale perspective. *J. Energy Eng.* 150 (2), 04024002. doi:10.1061/JLEED9.EYENG-5226

Teng, T., Wang, Y. M., Li, Z. L., Gao, Y. N., and Zhu, X. Y. (2023). Contrastive analysis of energy evolution in the tension and compression deformation processes of dry and water-saturated sandy mudstone. *J. Min. and Saf. Eng.* 40 (01), 174–183. doi:10.13545/j.cnki.jmse.2021.0633

Wang, C., and Wang, J. (2021). Effect of heterogeneity and injection borehole location on hydraulic fracture initiation and propagation in shale gas reservoirs. *J. Nat. Gas Sci. Eng.* 96, 104311. doi:10.1016/j.jngse.2021.104311

Wang, H. L., Xu, W. Y., Shao, J. F., and Skoczylas, F. (2014). The gas permeability properties of low-permeability rock in the process of triaxial compression test. *Mater. Lett.* 116, 386–388. doi:10.1016/j.matlet.2013.11.061

Wang, Y. L., Zhang, J. G., Sun, Y. W., and Cheng, Y. F. (2019). Study on effect of working fluid on fracture propagation and mechanical properties of shale: based on response surface methodology. *Fresenius Environ. Bull.* 28 (4A), 3511–3515.

Wang, H. X., Zhang, B., Wang, L., Yu, X., Shi, L., and Fu, D. (2020). Experimental investigation on the long-term interactions of anhydrite rock, crude oil, and water in a mine-out space for crude-oil storage. *Eng. Geol.* 265, 105414. doi:10.1016/j.enggeo.2019.105414

Wang, H. Y., Yang, S. G., Zhang, L. P., Xiao, Y., Su, X., Yu, W., et al. (2024). Experimental analysis of the mechanical properties and failure behavior of deep coalbed methane reservoir rocks. *Processes* 12 (6), 1125. doi:10.3390/pr12061125

Wu, J. Y., Wong, H. S., Zhang, H., Yin, Q., Jing, H., and Ma, D. (2024). Improvement of cemented rockfill by premixing low-alkalinity activator and fly ash for recycling gangue and partially replacing cement. *Cem. Concr. Compos.* 145, 105345. doi:10.1016/j.cemconcomp.2023.105345

Wu, Q. Q., Shi, L., Zhang, L. W., and Li, X. (2024). Effect of pore-bearing fluids on the mechanical behavior of siliceous cemented sandstones containing different clay contents and types. *Geoenergy Sci. Eng.* 240, 213058. doi:10.1016/j.geoen.2024.213058

Wu, J. Y., Yang, S., Williamson, M., Wong, H. S., Bhudia, T., Pu, H., et al. (2025a). Microscopic mechanism of cellulose nanofibers modified cemented gangue backfill materials. *Adv. Compos. Hybrid Mater.* 8, 177. doi:10.1007/s42114-025-01270-9

Wu, J. Y., Zhang, W. Y., Wang, Y. M., Ju, F., Pu, H., Riabokon, E., et al. (2025b). Effect of composite alkali activator proportion on macroscopic and microscopic properties of gangue cemented rockfill: experiments and molecular dynamic modelling. *Int. J. Minerals Metallurgy Mater.* 32 (8), 1813–1825. doi:10.1007/s12613-025-3140-8

Xu, K., Zhang, H., Zhang, Z. Z., Yin, G., Shang, X., Wang, Z., et al. (2023). Damage evolution characteristics of heterogeneous fractured sandstone reservoir under different fracturing fluids. *Energy Sci. and Eng.* 11 (10), 3447–3461. doi:10.1002/ese3.1532

Xu, W. H., Wang, Z. H., Shen, Z. F., Gao, H. m., Liu, Y. q., and Zhang, X. l. (2024). Simulation of saturated sand site liquefaction based on the CFD-DEM method. *Rock Soil Mech.* 45 (08), 2492–2501. doi:10.26599/rsm.2024.9436461

Yang, B., Wang, H. Z., Wang, B., Yi, Y., Zhao, C., and Tian, G. (2023). Effect of supercritical CO2-water/brine-rock interaction on microstructures and mechanical properties of tight sandstone. *Transp. Porous Media* 149 (1), 87–115. doi:10.1007/s11242-022-01834-z

Yao, J., Wang, C. Q., Huang, Z. Q., Zhou, X., and Li, J. L. (2024). Stress sensitivity of ultra-deep tight sandstone gas reservoirs based on microscopic fluid-solid coupling. *Nat. Gas. Ind.* 44 (5), 45–55. doi:10.3787/j.issn.1000-0976.2024.05.004

Yin, S., Zhang, Z. Y., Wang, R. Y., Liu, H. L., Xu, Z. Q., Wang, M. J., et al. (2025). Research progress, challenges, and prospects of reservoir geomechanics in deep and ultradeep oil and gas in China. *Nat. Gas. Ind.* 45 (4), 33–47. doi:10.3787/j.issn.1000-0976.2025.04.003

Yu, Y. J., Liu, J. M., Yang, Y. T., Song, Z. Y., and Zhao, S. Q. (2024). Mechanical properties and damage constitutive model of coal with different water content based on energy principle. *Coal Sci. Technol.* 52 (6), 67–80. doi:10.12438/cst.2023-1871

Zhang, S., Zhang, D. S., Wang, Z., and Chen, M. (2018). Influence of stress and water pressure on the permeability of fissured sandstone under hydromechanical coupling. *Mine Water Environ.* 37 (4), 774–785. doi:10.1007/s10230-018-0540-2

Zhang, Z. Z., Niu, Y. X., Shang, X. J., Liu, X., and Gao, F. (2021a). Characteristics of stress, crack evolution, and energy conversion of gas-containing coal under different gas pressures. *Geofluids* 2021, 1–18. doi:10.1155/2021/5578636

Zhang, Z. Z., Niu, Y. X., Shang, X. J., Ye, P., Zhou, R., and Gao, F. (2021b). Deterioration of physical and mechanical properties of rocks by cyclic drying and wetting. *Geofluids* 2021, 1–15. doi:10.1155/2021/6661107

Zhang, K., Liu, Y. X., Sheng, L. Q., Li, B., Chen, T., Liu, X., et al. (2022). Study on the effect of fracturing fluid on the structure and mechanical properties of igneous rock. *ACS Omega* 7 (14), 11903–11913. doi:10.1021/acsomega.1c07386

Zhang, C., Wang, X. J., Shi, X. T., Zhao, Y. X., Han, P. H., and Zhang, T. (2024). Splitting characteristics of sandstone under the influence of water saturation and its mechanism of water rock interaction. *Chin. J. Rock Mech. Eng.* 43 (S2), 3722–3737. doi:10.13722/j.cnki.jrme.2023.0352

Zhao, K., Yang, D., Zeng, P., Huang, Z., Wu, W., Li, B., et al. (2021). Effect of water content on the failure pattern and acoustic emission characteristics of red sandstone. *Int. J. Rock Mech. Min. Sci.* 142, 104709. doi:10.1016/j.ijrmms.2021.104709

Zhong, Y., Kuru, E. G., Zhang, H., Kuang, J., and She, J. (2019). Effect of fracturing fluid/shale rock interaction on the rock physical and mechanical properties, the proppant embedment depth and the fracture conductivity. *Rock Mech. Rock Eng.* 52 (4), 1011–1022. doi:10.1007/s00603-018-1658-z